The Astrophysical Journal, 596:1295–1304, 2003 October 20

THE UNUSUAL 2001 PERIASTRON PASSAGE IN THE "CLOCKWORK" COLLIDING-WIND BINARY WR 140

S. V. Marchenko[1]
Department of Physics and Astronomy, Western Kentucky University, Bowling Green, KY 42101-3576; sergey@astro.wku.edu

A. F. J. Moffat
Département de Physique, Université de Montréal, C.P. 6128, Succ. "Centre-Ville," Montréal, QC H3C 3J7, Canada; and Observatoire du mont Mégantic; moffat@astro.umontreal.ca

D. Ballereau and J. Chauville
GEPI, UMR 8111 du CNRS, Observatoire de Paris-Meudon, 92195 Meudon, France; dominique.ballereau@obspm.fr, jacques.chauville@obspm.fr

J. Zorec
Institut d'Astrophysique de Paris, CNRS, 98bis boulevard Arago, 75014 Paris, France; zorec@iap.fr

G. M. Hill
W.M. Keck Observatory, 65-1120 Mamalahoa Highway, Kamuela, HI 96743; ghill@keck.hawaii.edu

K. Annuk
Tartu Observatory, EE 2444, Toeravere, Estonia; annuk@aai.ee

L. J. Corral
Instituto de Astrofísica de Canarias, 38200 La Laguna, Tenerife, Spain; lcorral@ll.iac.es

H. Demers
Département de Physique, Université de Montréal, C.P. 6128, Succ. "Centre-Ville," Montréal, QC H3C 3J7, Canada; and Observatoire du mont Mégantic; hdemers@astro.umontreal.ca

P. R. J. Eenens
Department of Astronomy, University of Guanajuato, 36000 Guanajuato, GTO, Mexico; eenens@astro.ugto.mx

K. P. Panov
Institute of Astronomy, Bulgarian Academy of Sciences, Sofia, Bulgaria; kpanov@libra.astro.bas.bg

W. Seggewiss
Sternwarte der Universität Bonn, Auf dem Hügel 71, 53121 Bonn, Germany; seggewis@astro.uni-bonn.de

J. R. Thomson
David Dunlap Observatory, P.O. Box 360, Station A, Richmond Hill, ON L4C 4Y6, Canada; jthomson@crux.astro.utoronto.ca

and

A. Villar-Sbaffi
Département de Physique, Université de Montréal, C.P. 6128, Succ. "Centre-Ville," Montréal, QC H3C 3J7, Canada; and Observatoire du mont Mégantic; alfredo@astro.umontreal.ca
Received 2003 April 23; accepted 2003 July 1

ABSTRACT

We follow, using both optical spectroscopy and photometry, the "textbook" colliding-wind WR+O binary WR 140 through and between the periastron passages of 1993 and 2001. An extensive collection of high-quality spectra allows us to derive precise orbital elements for both components simultaneously. We confirm the extremely high eccentricity of the system, $e = 0.881 \pm 0.005$, find an excellent match of the newly derived period to the previous estimates, $P = 2899.0 \pm 1.3$ days, and improve the accuracy of the time of periastron passage, $T_0 = \mathrm{HJD}\ 2,446,147.4 \pm 3.7$. Around periastron, at orbital phases $\phi \sim 0.995$–1.015, additional emission components appear on the tops of the broad Wolf-Rayet emission lines of relatively low ionization potential. The phase-dependent behavior of these excess line emissions points to their origin in the wind-wind collision zone, which allows us to place some limits on the orbital inclination of the system, $i = 50° \pm 15°$, and half-opening angle of the bow shock cone, $\theta = 40° \pm 15°$. The relatively sudden appearance and disappearance of the extra emission components probably signify a rapid switch from an adiabatically to a radiatively dominated regime and back again. Multiyear *UBV* photometry provides one more surprise: in 2001 at $\phi = 0.02$–0.06, the system went through a series of rapid, eclipse-like events. Assuming these events to be related to an episode of enhanced dust formation at periastron, we estimate the characteristic size of the dust grains to be $a \sim 0.07\ \mu$m.

Subject headings: binaries: spectroscopic — stars: early-type — stars: individual (WR 140) — stars: Wolf-Rayet

On-line material: machine-readable tables

[1] Formerly at Département de Physique, Université de Montréal, Montréal, QC, Canada.

1. INTRODUCTION

The long-period massive Wolf-Rayet (WR) binary HD 193793 (WR 140) is frequently considered a textbook example of the colliding-wind phenomenon. The binary consists of a carbon-sequence Wolf-Rayet (WC7) star orbiting a more massive and luminous O4-5 main-sequence companion. The system's high eccentricity and rather favorable inclination help to probe different regions of the Wolf-Rayet wind and, at the same time, the profound change of conditions in the wind-wind collision zone at the times of periastron passage. This change is mainly reflected in rapid formation of dust clouds and can be detected as gigantic IR outbursts occurring on a strictly periodic (once per orbit) timescale (see Williams et al. 1990 for unresolved IR photometry, and Monnier, Tuthill, & Danchi 2002 for direct IR imaging).

The status of the system as a strong nonthermal, variable radio source (Williams, van der Hucht, & Spoelstra 1994), as well as an extremely bright (for a WR star) X-ray source (Pollock, Haberl, & Corcoran 1995) makes WR 140 an ideal laboratory for studying the properties of hot stellar winds (White & Becker 1995). The almost perfectly phase-dependent behavior of the system in radio and X-rays is remarkable. Many times over the past decade, WR 140 has been a target for long-term multiwavelength campaigns with subsequent state-of-the-art modeling of the colliding-wind phenomenon (see numerous reports in van der Hucht & Williams 1995; Zhekov & Skinner 2000). In 1999–2002 we intensified our large optical campaign in an attempt to follow the system with shorter time steps through the 2001 periastron passage. To our surprise, the "clockwork" behavior of WR 140 changed dramatically during its periastron passage in 2001. Below we report on this spectroscopic and photometric monitoring and provide a brief interpretation of the results.

2. OBSERVATIONS

Our new data set consists of two parts. The first part comprises high signal-to-noise ratio (S/N), moderate-to-high resolution CCD (some RETICON as well) spectra collected over the last two orbital cycles, 1986–2001. For revision of the orbital parameters and to search for rapid spectral variability, we used the spectra obtained at six different sites (Table 1): Observatoire de Haute-Provence (OHP; France), the Dominion Astrophysical Observatory (DAO; British Columbia, Canada), the David Dunlap Observatory (DDO; Ontario, Canada), the Mont Mégantic Observatory (OMM; Québec, Canada), the Ritter Observatory (RO; Ohio), and the San Pedro Martir Observatory (SPM; Baja California, Mexico).

All the spectra were initially processed using standard IRAF[2] tasks for bias subtraction, flat-field division, sky subtraction, spectrum extraction, and wavelength calibration. We paid particular attention to the rectification procedure, selecting in every spectrum precisely the same relatively line-free regions and approximating the continuum shape by a low-order polynomial. This allowed us to reach an acceptable $\lesssim 2\%$ accuracy when measuring intensities of the emission features in the individual spectra. The achieved accuracy was mainly limited by the extreme width of the emission profiles in question, as well as by the scarcity of line-free regions in the optical spectrum of WR 140.

The second part of the new data set includes long-term *UBV* (Johnson) photometric observations obtained at two sites:

1. The 60 cm telescope of the National Astronomical Observatory Rozhen (Bulgaria) equipped with a single-channel, photon-counting photometer (for additional details see Panov, Altmann, & Seggewiss 2000; HD 193888 was used as the comparison and HD 193926 as the check star), providing an average accuracy of 0.003–0.005 mag per point, each point usually representing an average of 3–5 consecutive observations separated by intervals of a few minutes. In the discussion we use the previously described data from the 1991–1998 campaign, along with the newly acquired photometry from 1999–2001 (Table 2; see also a preliminary report in Panov & Dimitrov 2001).
2. The automatic 25 cm telescope in Arizona (Young et al. 1991), delivering one data point per night and running since 1992 September. Use of HD 192934 and HD 192985 as the check and comparison stars, respectively, provided a precision of 0.008 mag in *B* and *V* and 0.009 mag in *U* over the whole period of observations. In Table 2 we list the heliocentric Julian date of observations and the WR-comp values in *U*, *B*, and *V*, starting from the Rozhen Observatory set and concluding with the automatic telescope data (APT).

3. RESULTS

3.1. *Spectroscopy*

Good time coverage of the last two periastron passages with high-quality spectral data allows us for the first time to provide a consistent, simultaneous orbital solution based on the radial velocities (RVs) of both components. To secure

[2] IRAF is distributed by the National Optical Astronomy Observatory, operated by the Association of Universities for Research in Astronomy, Inc., under cooperative agreement with the National Science Foundation.

TABLE 1
SPECTRAL OBSERVATIONS OF WR 140

Observatory	Telescope	Dates	Number of Spectra	Spectral Coverage (Å)	Spectral Resolution (Å pixel^{-1})	S/N (continuum)
OHP	1.5 m	2000 Nov–2001 Aug	16	5220–5990	0.22	340 ± 120
DAO	1.2 m, 1.8 m	1986 Aug–1997 Jul	24	5080–6140	0.48	340 ± 90
DDO	1.9 m	2001 Jan–2001 Mar	7	5410–6060	0.62	260 ± 100
OMM	1.6 m	1986 Jan–2001 Feb	90	4200–6580	0.44–0.66	290 ± 160
RO	1.0 m	2001 Feb–2001 Apr	3	5240–6240	1.56–1.62	110 ± 10
SPM	2.1 m	2000 Apr, 2001 Jun	2	3600–6900	0.18	300–400

TABLE 2
UBV Photometry of WR 140 in 1991–2002

HJD−2,400,000	WR-c V	WR-c B	WR-c U
Rozhen Observatory			
51428.425	−1.676	−1.265	−1.373
51447.347	−1.680	−1.261	−1.364
51448.341	−1.686	−1.269	−1.378
51452.328	−1.679	−1.267	−1.376
51453.309	−1.680	−1.268	−1.380
51454.318	−1.690	−1.272	−1.386
51455.322	−1.690	−1.268	−1.382
51700.536	−1.690	−1.260	−1.385
51701.514	−1.707	−1.269	−1.390
51702.510	−1.685	−1.256	−1.361
51704.501	−1.688	−1.274	−1.392

Note.—Table 2 is published in its entirety in the electronic edition of the *Astrophysical Journal*. A portion is shown here for guidance regarding its form and content.

the highest possible precision, we used the deep and narrow interstellar (IS) Na I absorption lines as "fiducial marks" to tweak the RVs of WR 140 by co-aligning all the available spectra based on this IS line pair. As an additional check we also used the less prominent diffuse IS bands at 5780 and 5797 Å. This approach substantially reduced systematic differences between the various subsets of data, bringing them down to $\Delta(\mathrm{RV}) \lesssim 5$ km s^{-1}. Then we constructed an average spectrum of WR 140 using practically all newly acquired spectra (omitting those at phases 0.00 ± 0.02 around periastron passage; see below) and supplementing them by the large collection of high-quality CCD spectra obtained at the Mont Mégantic Observatory in 1989–1994 and described by Hervieux (1995)—again neglecting those spectra close to periastron.

We measured the RVs of the WR component by cross-correlating individual spectra with the template in the range of either 5360–5950 Å for the majority of the available data, or 4280–4900 Å for a few spectra from the 1989–1994 Mont Mégantic collection. RVs of the O star were obtained by measuring centroids of the He II 5412, O III 5696, and He I 5876 Å absorptions (Hγ, He II 4542, and Hβ in the blue-green region) and averaging them with equal weights. Table 3 lists the heliocentric Julian dates along with the RVs ($\pm\sigma$) for the WR and O components, observatory by observatory. To find reliable orbital elements, we used in addition to the data from Table 3, the measurements (for both components) described by Annuk (1995) along with the RVs of the O component from Lamontagne et al. (1984), Conti et al. (1984), Moffat et al. (1987), and Setia Gunawan et al. (2001).

TABLE 3
Radial Velocities of the WR and O Components of WR 140

HJD−2,400,000	Observatory	RV(WR) $\pm\sigma$ (km s^{-1})	RV(O) $\pm\sigma$ (km s^{-1})
46658.8106	DAO	10.6 ± 5.4	-16.3 ± 6.4
47004.8665	...	14.3 ± 5.3	-0.1 ± 6.8
47025.8566	...	13.0 ± 7.8	8.8 ± 11.2
47083.6879	...	13.1 ± 3.8	-26.7 ± 6.5
47365.8505	...	10.1 ± 7.4	-1.3 ± 7.9
47391.7946	...	12.3 ± 4.8	-2.4 ± 5.6
48114.7750	...	-5.2 ± 3.3	6.1 ± 4.5
48131.7955	...	-12.1 ± 6.2	7.4 ± 4.4
48133.7368	...	-9.1 ± 4.7	4.9 ± 2.5
48505.8792	...	-22.8 ± 6.6	-10.2 ± 28.0

Note.—Table 3 is published in its entirety in the electronic edition of the *Astrophysical Journal*. A portion is shown here for guidance regarding its form and content.

TABLE 4
Orbital Elements of WR 140

Element	WR	O
K (km s^{-1})	82.0 ± 2.3	30.5 ± 1.9
$a \sin i$ (10^{10} km)	0.154 ± 0.007	0.057 ± 0.004
γ	assumed: 0.0	3.1 ± 1.0
P (days)	2899.0 ± 1.3	...
e	0.881 ± 0.005	...
T_0 (HJD 2,440,000+)	6147.4 ± 3.7	...
ω	46.7 ± 1.6	...

The combined data set (206 RV measurements for the WR component and 280 estimates for the O star) was fitted using the algorithm of Bertiau & Grobben (1969). We have assigned equal weights to all the fitted data. Before combining the data from different sites into a uniform system of RVs, we found a preliminary solution treating each subset separately, with the systemic velocities of the WR and O components as free parameters. Then, each subset with a significant ($>2\ \sigma$) deviation of the systemic velocities was shifted to conform with the DAO+OMM frame of reference, i.e., to match the most representative and uniform subsets of data covering almost three orbital cycles. Application of an alternative fitting procedure developed by one of us gave similar results. The best fit provides an average precision of $\sigma_{O-C}(\mathrm{RV}) = 13.2$ km s^{-1}, which exceeds the accuracy of the individual measurements from Table 3. However, this discrepancy must also allow for the lower accuracy of the O-star measurements extracted from the literature, as well as the inhomogeneity of the data set.

We list the orbital parameters along with the corresponding errors in Table 4, and plot the data from Table 3 along with the best orbital fit in Figure 1. Within the errors, the

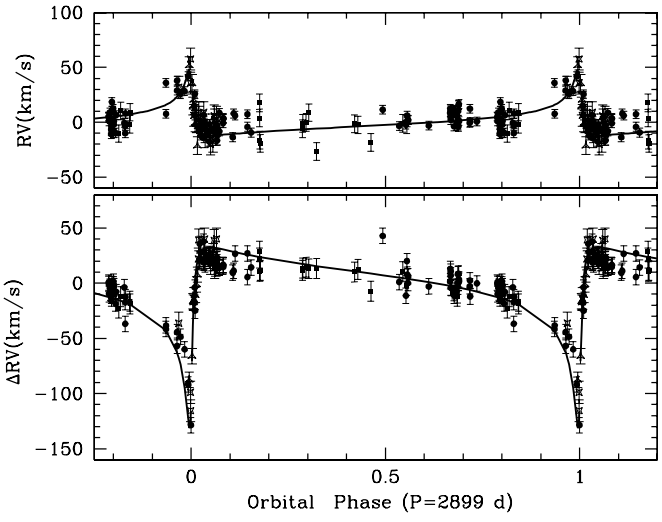

Fig. 1.—Orbits of the O (upper panel) and WR (lower panel) components of WR 140. Different symbols depict: *filled squares*, DAO data; *filled circles*, OMM data; *open triangles*, DDO data; *open squares*, OHP data, all with corresponding $\pm\sigma$ error bars.

newly derived orbital period perfectly matches the estimate of Williams et al. (1990), which was based on the repetitive episodes of dust formation. Our value of the eccentricity is slightly higher than that quoted in previous studies, but still well within the uncertainties. The RV amplitudes of the WR and O components also match well the earlier derived values.

Searching for signs of spectral variability of the WR component, we find the emission line profiles to be stable over all orbital phases except the relatively brief period around periastron passage, $\phi = 0.005 \pm 0.015$. This phenomenon was first reported by Hervieux (1995). Only two lines, both of low ionization potential, C III 5696 and He I 5876, show clear signs of variability. To highlight these rapid changes, we first create an overall mean WR profile by collecting all the available spectra (except those around periastron passage), shifting them by the orbital motion of the WR component and, finally, averaging them. Then we subtract the mean, appropriately shifted spectrum from the individual spectra in the WR frame, bin the differences to 0.01 (phases $0.01 < \phi < 0.99$) or 0.005 (phases 0.00 ± 0.01) phase bins and plot the phase-binned differences in Figure 2. With notable consistency in both lines, a broad extra emission component appears on the blue side of the WR profile at $\phi \sim 0.99$, quickly migrates to the red side, and disappears at $\phi \sim 1.02$. Comparing the spectra taken during two recent periastron passages, we find this phenomenon repeatable and phase-locked. One may also note the line profile variations especially clearly seen in C III at $v \sim \pm 2500$ km s^{-1}. They are probably linked to the differences in spectral resolution of the various data subsets (note that the variability is limited to the relatively narrow spectral regions corresponding to the steep flanks of the emission lines). However, in some cases the seemingly stochastic, rapid (night-to-night) variability of the P Cygni absorption component contributes to the problem as well. It remains to be seen whether this random variability is related to the enhanced interaction between the stars during periastron passage (note that it happens between phases 0.00 and 0.02).

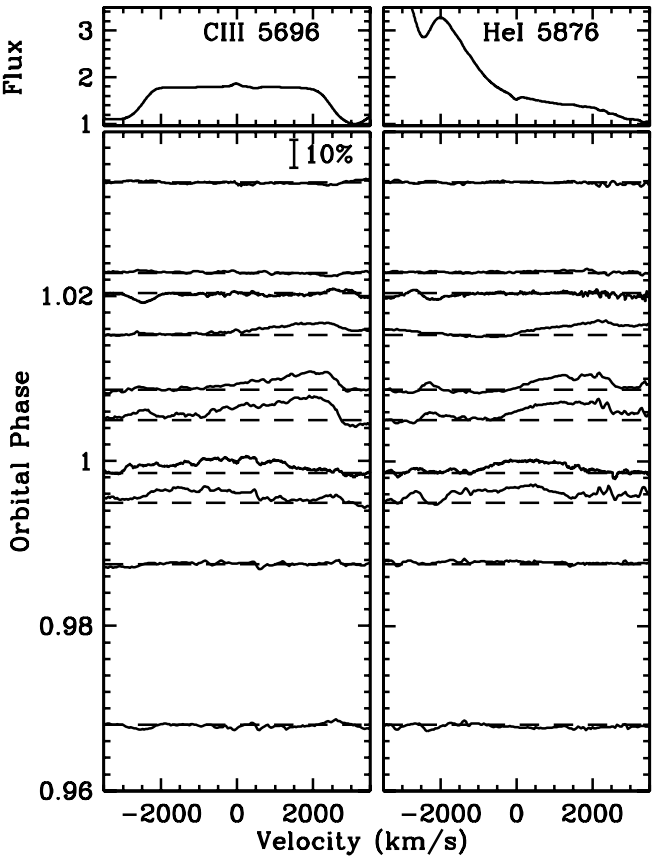

FIG. 2.—Rapid, phase-locked variability seen in the lines with low ionization potential. Phase-binned differences between the individual and mean profiles are shown by solid lines. Dashed lines mark zero levels for each bin.

3.2. *Photometry*

Our long-term, two-site *UBV* monitoring of WR 140 has brought a surprise. To study the long-term variably of the system, we merge the observations collected by the Rozhen Observatory and APT by shifting the zero points of the former to match the average magnitudes of the APT measurements between HJD 2,450,000 and 2,451,800 (note that in Table 2 we give the Rozhen data in their original form). We plot the combined data set in Figure 3. During the 1993 periastron passage, Panov et al. (2000) detected only a shallow, $\Delta V \sim 0.03$, broad minimum and interpreted this as related to the episode of dust formation. The simultaneous 1993 APT photometry confirmed the slight dimming of the star after periastron passage, additionally pointing to a higher photometric activity during this period of time; note the higher scatter in the V measurements around HJD 2,449,200 (Fig. 3, *upper panel*). Most remarkably, the behavior of the star changed radically during the 2001

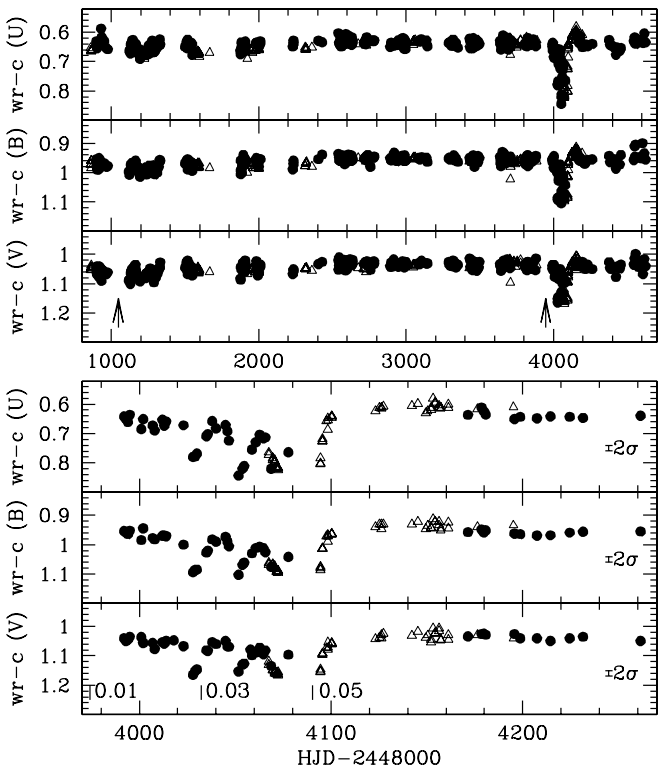

FIG. 3.—Two-site *UBV* monitoring of WR 140: *filled circles*, APT in Arizona; *open triangles*, Rozhen Observatory. Arrows mark the 1993 and 2001 periastron passages. Orbital phases along with 2 σ error bars are plotted in the lower section.

periastron passage. We found a series of quasi-regular fadings starting ~2.5 months after periastron passage and lasting ~2.5 months (Fig. 3, *lower panel*). They rapidly develop into a major fading event at $\phi \sim 0.05$, with a clearly color-dependent amplitude that increases toward shorter wavelengths.

4. DISCUSSION

4.1. *Wind-Wind Interaction Effects*

We first turn our attention to the rapid appearance of the extra emission components on the tops of the low-ionization lines of C III and He I around periastron. First detected in 1993 (Hervieux 1995), the same effect was observed in 2001, one orbital cycle later, in both the optical (this paper) and the near-IR lines (Varricatt, Williams, & Ashok 2003). All independent data sets show a blueshifted excess emission arising shortly before periastron and rapidly shifting to the red side of the underlying WR profile at more advanced phases. At least one other eccentric WR+O binary system, γ^2 Vel, shows an extra emission component on top of its C III 5696 line, whose intensity also varies with orbital separation (St-Louis 1996). A few dozen high-quality spectra taken during the critical orbital phases provide some interesting details.

We measure the integrated fluxes of the extra emission features in each difference spectrum (individual profile − average profile), normalize these fluxes by the maximum flux observed in C III, and plot them versus orbital phase and normalized orbital separation in Figure 4. The latter is calculated as $d = [d(\phi) - d_{\min}]/d_{\min}$, where $d(\phi)$ is the phase-dependent orbital separation and $d_{\min}$ is the separation at periastron, $\phi = 0$. There is a sharp rise toward a sharp peak in excess emission that occurs at phase 0.0013 after periastron for both lines, C III 5696 Å and He I 5876 Å, followed by a possibly slightly less steep decline. At its maximum, the extra emission component delivers 13% to the line's flux of C III and 8% of He I. The uncertainties of measurements of the fluxes can be assessed by looking at the scatter of points at $d > 1.5$ in Figure 4. The scatter, frequently negative, highlights the problems of the continuum rectification in the 5500–6000 Å spectral region, where the broad, intense lines of C III, C IV, and He I create a single blend (Fig. 5). Nevertheless, the amplitude of the peak at $d = 0$ greatly exceeds the uncertainties. The rapid redshift of the extra emission features hints at the origin of the emissions in the wind-wind collision (WWC) zone, which is supposedly located between the stars and wrapped around the O component (e.g., Stevens, Blondin, & Pollock 1992). Indeed, using the orbital elements of WR 140, one can reproduce, if only qualitatively, the observed shift: as the phase changes between $\phi = 0.98$ and 1.02, the O component quickly moves behind the WR star (see Fig. 2 in Setia Gunawan et al. 2001). Hence, the RVs of the excess emission component, emerging from the WWC zone downstream from the bow shock head, reflect this orbital motion and show a quick blue-to-red excursion.

In colliding wind systems, one expects the excess emission to vary in position and shape over the course of an orbital cycle. As shown by Lührs (1997; see also a similar approach in Neutsch et al. 1981), it often assumes a double-peaked profile. The positions of the two peaks are predicted to vary in a certain way with phase, depending mainly on the streaming velocity of material in the shock cone ($v_{\rm cone}$), the orbital inclination (i), the half-opening angle of the shock cone (θ), and the Coriolis-induced angular deviation of the cone's axis from the line joining the two stars ($\delta\phi$). In

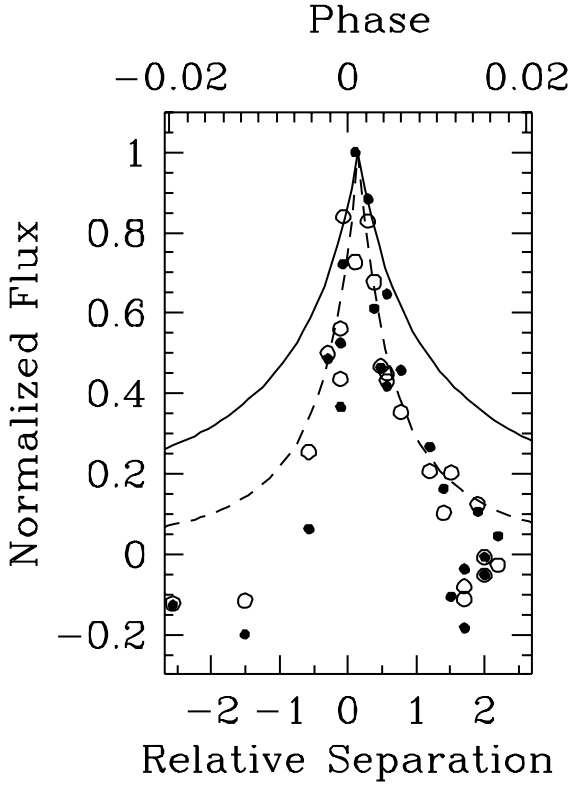

FIG. 4.—Normalized flux of the extra emission components in the C III line (*filled circles*) and the He I line (*open circles*) are plotted vs. orbital phase (upper axis) and normalized orbital separation d (lower axis). A d^{-1} dependence fitted to the peak of the extra flux is depicted by the solid line, and a d^{-2} dependence is traced by the dashed line.

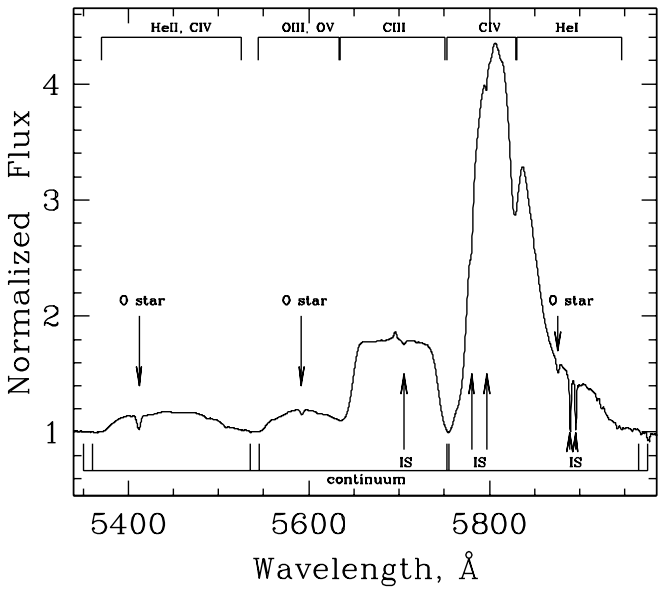

FIG. 5.—Mean spectrum of WR 140 based on constant spectra avoiding periastron passage. Bars at the top indicate the ranges of various WR emission lines. O-star photospheric absorption lines along with interstellar features are indicated. Continuum windows used for spectral rectification are shown by double vertical lines at the bottom.

principle, this means one can learn much about the system without detailed profile fitting. Depending on spectral resolution, and velocities and geometry of the shock cone, however, the double peaks might not be visible. Faced with this situation, one can still derive some valuable estimates of the colliding wind region by measuring the entire excess emission. Hill et al. (2000, 2002) have shown that the width and position of the excess emission vary as

$$\mathrm{FW_{ex}} = C_1 + 2v_{\mathrm{cone}} \sin\theta \sqrt{1 - \sin^2 i \cos^2(\phi - \delta\phi)} \ , \quad (1)$$

$$\mathrm{RV_{ex}} = C_2 + v_{cone} \cos\theta \sin i \cos(\phi - \delta\phi) \ , \quad (2)$$

where C_1 and C_2 are simple constants, and phase $\phi = 0.0$ has the Wolf-Rayet star in front.

Unlike the cases for WR 42, WR 48, and WR 79 described by Hill et al. (2000, 2002), we face additional complications here. The orbit is not circular, and we do not have full phase coverage. The first complication is overcome by fitting versus true anomaly in the orbit rather than phase. The second complication is not as bad as it appears at first, since the very limited phase over which excess emission is measurable corresponds to about 150 degrees of true anomaly.

Using equations (1) and (2), we have fitted the measurements of the width and position of the excess emission shown in Figure 2. Details of the fitting technique can be found in Hill et al. (2000). Reasonable fits are obtained for a very wide range of parameters, but some limits can be derived by making a few reasonable assumptions. For example, we can require that velocity of the gas streaming along the bow shock cone, v_{cone}, not exceed the terminal velocity of the WR wind, v_∞. Eenens & Williams (1994) find 2900 km s^{-1} for v_∞ for the WR star component of WR 140. Another possible constraint can be obtained by assuming that turbulence in the shock cone contributes to the constant C_1. Hill et al. (2002) found that numbers of the order of 200–500 km s^{-1} were appropriate for WR 42, WR 48, and WR 79 in this respect. Using these constraints, we obtain $v_{\mathrm{cone}} = 2300 \pm 500$ km s^{-1}, $i = 50^\circ \pm 15^\circ$, $\theta = 40^\circ \pm 15^\circ$, and $\delta\phi = 40^\circ \pm 20^\circ$. A fit using these parameters is shown in Figure 6. Applying the approach of Cantó, Raga, & Wilkin (1996), we find that $\theta = 40^\circ$ leads to $[\dot{M}(\mathrm{O})v_\infty(\mathrm{O})]/[\dot{M}(\mathrm{WR})v_\infty(\mathrm{WR})] = 0.045$, in a fair agreement with 0.028, the estimate of Williams et al. (1990); here $\dot{M}$ and v_∞ are the mass-loss rates and the terminal wind velocities of the WR and O components.

An even more intriguing feature is the extremely rapid rise and fall of the extra emission component. In general, for such a wide, long-period binary the WWC zone can be treated as adiabatic even at periastron (Stevens et al. 1992). Assuming the WWC excess emission detected in the C III and He I lines to be optically thin (a reasonable assumption for a subordinate line formed at $\sim 100 R_{\mathrm{WR}}$), we can expect to see a $\sim d^{-1}$ rise/fall of the emissivity (Usov 1992; Stevens et al. 1992). In the case of WR 140, the emission grows and falls off much more quickly, approximately as d^{-2} (Fig. 4). This may signify that the WWC zone experiences a rapid transition from an adiabatically governed state at large orbital separations to a radiatively driven emissivity around periastron passage, when the hot, cooling, compacted WWC gas boosts the emission measure of the zone. The quick growth of density in the WWC zone may greatly facilitate dust production, which regularly happens right after periastron passage, i.e., at phase 0.02–0.03. This small delay is likely linked to the travel time of the WR wind to where the dust is formed (Williams et al. 1990). The asymmetry in the rise/fall of the emission may arise when the orbital and free-flow timescales became compatible, which happens during periastron passage. Inability of the WWC zone to adjust to the rapidly changing boundary conditions causes a lag in the directly observable response (i.e., the fall-off rate of the extra emissivity) from the WWC zone. Indeed, hydrodynamical simulations (Walder & Folini 2003) clearly show a time delay in the reaction of the geometry of the WWC zone to the rapidly changing orbital separation.

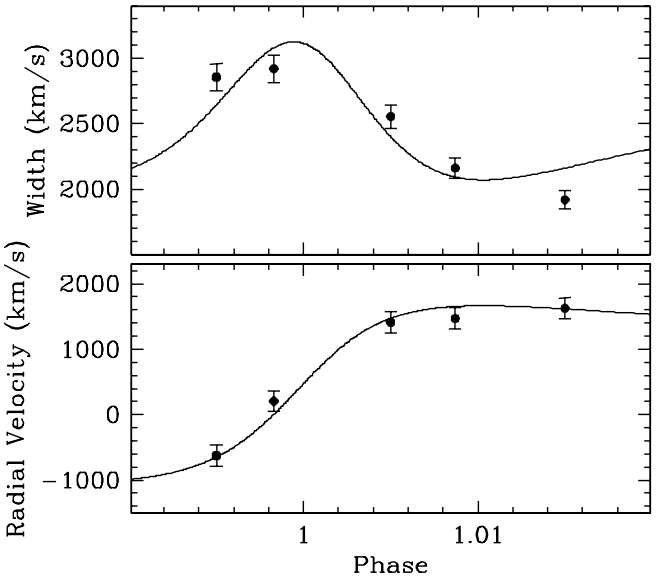

FIG. 6.—*Upper panel*: Fit to the FWHM of the excess emission (combined profiles of C III and He I lines). *Lower panel*: Fit to the radial velocity of the excess emission with corresponding $\pm\sigma$ error bars.

The phase shift of maximum excess emission to 0.0013 after periastron corresponds to 3.7 days, which is the same order as the uncertainty in T_0 (3.7 days). Nevertheless, a minimum delay (assuming a constant-velocity wind; for a more realistic β expansion law, this delay will be larger) close to 1 day is expected due to the finite travel time of the WR wind material (which forms the excess C III and He I emission lines) from the WR star (which determines the orbit) to the stagnation point in the WWC zone. This minimum may actually apply to the real delay if the winds are highly clumped. Otherwise, for a smooth, adiabatic wind, the time of maximum excess line emission will occur at about an orbital separation, i.e., $a(1 - e)$ at periastron, farther downstream along the shock cone (Folini & Walder 2002), i.e., with a total delay of $\sim$2 days after periastron.

4.2. *Anisotropy of the WR Wind?*

There is at least one alternative interpretation of the extra emission phenomenon. Analyzing the results of long-term, multiwavelength monitoring of the radio flux, White & Becker (1995) came to the conclusion that the wind of the WR component could be highly anisotropic, with its mass-loss confined mainly to its equatorial plane, which does not coincide with the orbital plane (see, however, the criticism of the model by Pollock et al. 2002). This plane is oriented in

such a way that the O star crosses it at $\phi \sim 0.7$ and 0.0. The first passage should not result in any enhancement of the emissivity of the subordinate lines in the optical because of the large separation of the components, while the passage happening around periastron may lead to the rapid growth of emissivity when the luminous, hot O star plunges into the densest part of the flattened WR wind. This point was reiterated by Zhekov & Skinner (2000) who, comparing the results of hydrodynamic modeling of the colliding winds in WR 140 to the observed X-ray spectra, found that near periastron the fitted results can be significantly improved by introducing an extra absorption, well above that expected from the winds and interstellar medium. This may signify the presence of a flattened, disklike structure tilted relatively to the orbital plane.

We address this hypothesis by trying to reproduce the behavior of the intrinsic linear polarization in an eccentric WR+O binary in which the WR component may have an equatorially enhanced wind. Previous long-term optical polarimetric monitoring (Whitney et al. 1988) shows a small, $\sim$0.1%, but significant decrease of polarization over the 2 years after periastron passage. However, the (linear) polarization spectrum of the system appears to be featureless (Schulte-Ladbeck 1994;[3] Harries, Hillier, & Howarth 1998), i.e., bearing no signs of the possible flattening of the WR wind.

We developed a polarimetric model to simulate the polarization caused by electron scattering in the wind of the WR star. Assuming a rotationally enhanced mass-loss rate, we reproduced a disklike wind resembling the one proposed by White & Becker (1995). We calculate the net polarization as the sum of a constant contribution from the WR star illuminating its own anisotropic wind, and the O star producing a variable phase-locked component as it orbits around the WR star and illuminates different parts of the inhomogeneous WR wind. This model does not take into account the wavelength-dependent interstellar component that is to be added to the net polarization.

We used a Monte Carlo method to evaluate the integrals describing the polarization in the linear Stokes parameters Q and U as a function of the binary light curve phase (Robert et al. 1990) that we adapted to take into account an eccentric orbit. These integrals assume an optically thin wind corotating in the frame of the binary and are usually referred to as BME approximations (see Brown, McLean, & Emslie 1978).

Each integration is carried out in a spherical region around the WR star, and each point is chosen using a Sobol quasi-random number sequence in three dimensions with a word length of 30 bits. The anisotropy is introduced by assuming the rotationally enhanced mass-loss rate from Friend & Abbott (1986), which is frequently used in evolutionary models (Maeder & Meynet 2000):

$$\dot{M}(\alpha, \delta) = \dot{M}(\alpha = 0)\left(\frac{1}{1 - \alpha \sin \delta}\right)^{0.43}, \qquad (3)$$

where α is the ratio of the rotational velocity at the equator to the critical breakup velocity and δ is the latitude measured from the pole. The electron density is calculated using the principle of mass conservation at every point in the accelerated wind by assuming a β-type velocity law with $\beta = 1.0$. We use a simplifying assumption that the WR wind consists exclusively of ionized helium, thus following the prescriptions of Moffat & Marchenko (1993) for a typical WNE star with $R_* = 3\ R_\odot$. Although this might not be directly applicable to the case of a WC star like WR 140, we use the simplified radial distribution of electron density as a first-order approximation. We expect any discrepancy only at the outer regions of the wind, where the contribution to the total polarization is minimal.

The orbital parameters for the model are taken from Table 4. We adopt an orbital inclination of $i = 60°$, resulting from the best fit of Williams et al. (1990) to the X-ray–absorbing column density. This value is comparable to our estimate derived from the fits to the extra emission components (see above). We also account for the difference in luminosity of the WR and O components (Williams et al. 1990). The mass-loss rate at the poles [i.e., $\dot{M}(\alpha = 0)$] and the terminal velocity of the wind of the WR star were taken from Zhekov & Skinner (2000, their model A). Although our model can take into account the finite size of the stars, we have neglected this effect, since the considered orbital separations are much larger than the sizes of the stars. We have also neglected light attenuations caused by any kind of eclipse-like phenomena, since their amplitude is relatively low (see Panov, Altmann, & Seggewiss 2000 and this paper) and would not significantly affect our results.

With this model, we performed three types of simulations in order to determine the effect of a flattened wind on the observed polarization. We started from a standard case of a spherically symmetric wind with $\alpha = 0$. The result of this first model (model 1) is presented in Figure 7.

Then, we simulated the case of a disklike wind by applying $\alpha = 0.95$ (model 2). This resulted in a density ratio

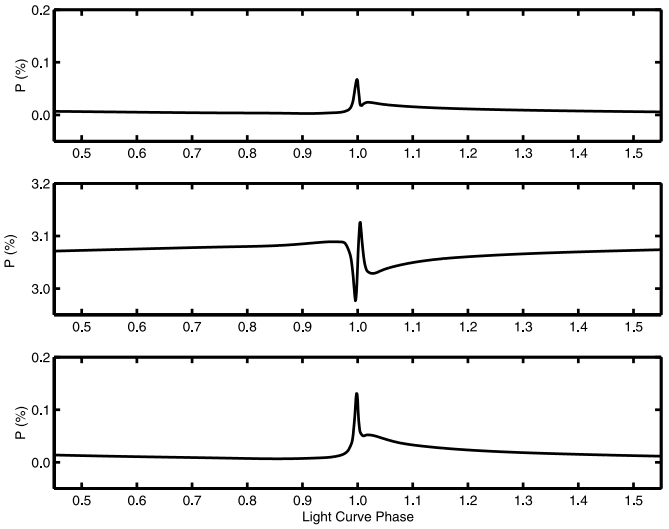

FIG. 7.—Simulated polarization as a function of orbital phase for the binary WR 140. The top panel shows the case of a spherically symmetric wind; the middle and bottom panels present the case of a rotationally flattened WR wind with an equator-to-pole density ratio of $\sim$3.6 and an orientation for the wind's equatorial plane corresponding to the model proposed by White & Becker (1995). In the middle panel, the initial orientation of the equatorial plane of the WR wind is coplanar with the orbital plane; in the bottom panel, the equatorial plane is initially oriented in the plane of the sky (see text for more details).

[3] The results can be accessed at: http://www.sal.wisc.edu/HPOL/gif/WR140.gif and www.sal.wisc.edu/HPOL/tgts/WR140.html.

between the equator and the poles of ~3.6. We introduced a rectangular system of coordinates with the X-axis pointing to the observer and the Y-axis going along the orbital plane (note the similarity of our approach to the scheme introduced by Brown et al. 1982). We oriented the orbital plane at the $i = 60°$ angle measured in the $X0Z$ plane from the Z-axis. Initially, the equatorial plane of the WR wind (hereafter "the disk") was made coplanar with the orbital plane. We aimed to reproduce the configuration suggested by White & Becker (1995), in which the O star crosses the high-density parts of the WR disk at orbital phases 0 and 0.7. This requires a rotation of the WR disk by 106° in the $Y0Z$ plane.

For the third case (model 3), we have chosen a pole-on initial orientation of the flattened WR wind with $\alpha = 0.95$, with subsequent rotation of the disk in the $X0Y$ plane by 52°.5. This allows the O star to cross the disk at $\phi = 0.7$. This configuration seems to be less likely to occur than the previous model. Defending our choice, we note that, considering an extremely high eccentricity, the tidally induced synchronization of the orbital motion and axial rotation (Zahn 1977) seems not to have much influenced the initial orbit and rotation of the components of WR 140. This may be a natural consequence of the long orbital period, as synchronization is proven to be efficient in systems with $P \lesssim 250$ days (De Medeiros, Da Silva, & Maia 2002). On the other hand, there is no reason to expect coplanarity of the rotational and orbital planes in an asynchronous eccentric binary (Stawikowski & Glebocki 1994). Note also that any deviation from the initially imposed pole-on orientation of the disk would lead to a rapid increase of the intrinsic polarization component, similar to model 2.

As expected for all cases, the amplitude of the polarimetric variability is very low (Fig. 7) and probably below or close to the limits of detection in the previous studies. However, the constant, wavelength-independent contribution from the WR star to the polarization in model 2 (about 3%) seems to be much too high and would have been detected by Schulte-Ladbeck (1994) and Harries et al. (1998) in the spectropolarimetric data even if no variability was discovered. This is a potential serious drawback for the model of an equatorially enhanced wind. However, the problem could be resolved if one accepts the configuration of model 3, no matter how unlikely seems the requirement that the WR disk be almost perpendicular to the orbital plane.

4.3. *Photometric Variability*

Now we turn to the photometric behavior of the system during periastron passage in 2001. If either of the stars, WR or O, is responsible for the seemingly periodic episodes of fadings, then, considering the amplitudes of the changes, one might expect that such drastic variability in the continuum light (noting that the emission lines contribute ~16% of the flux in V) should be accompanied by detectable line profile variability. We already mentioned that any variability of the WR emissions subsides at $\phi > 0.015$, i.e., long before the main fading episode (Fig. 3, *lower panel*). The contemporaneous O star profiles show no detectable changes either. To demonstrate this, we plot the individual O-star profiles in Figure 8 using the corresponding average profiles of He II 5412 and He I 5876 as a rough guideline. These averages were constructed from all the available spectra, including the lower resolution spectra from the OMM collection. Hence, the overall average profiles look shallower than the spectra from the sequences obtained at OHP and DDO. Allowing for this, we see that the O-star profiles do not change significantly with phase.

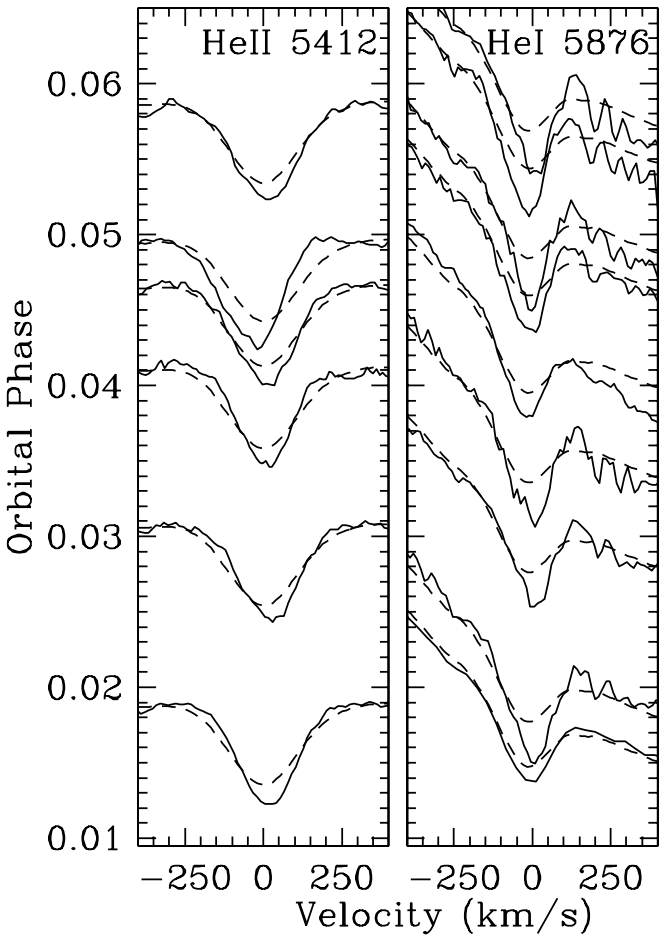

FIG. 8.—Individual absorption line profiles of the O star (*solid lines*) and the corresponding average absorption profiles (*dashed lines*) sorted with increasing orbital phase.

An alternative explanation relates the fading episodes to the dust formation phenomenon. The system is famous for its repetitive IR outbursts happening during periastron passage. The steeply rising, then slowly fading IR flux was linked to the formation of the hot, radiating dust cloud emerging from the WWC zone (Williams et al. 1990). The diffraction-limited 2.2 μm images from the Keck I telescope captured the dust cloud formed during the 2001 periastron passage (Monnier, Tuthill, & Danchi 2002). The images show a dust plume that slowly recedes from the system. In addition to the plume, there are a handful of bright clumps. They were reidentified in the images taken at the William Herschell Telescope a few months later (P. Williams 2002, private communication), thus giving additional weight to all the fine details seen in the Keck images. The behavior of the H flux (Williams et al. 1990) indicates that dust formation starts at $\phi \sim 0.00$ and proceeds with an increasing pace at least until $\phi \sim 0.03$. Considering the proper motions of the dust clumps (see Fig. 1 from Monnier et al. 2002), there is a high probability that some dust patches have caused the eclipsing-like behavior of the system in the optical. If true, then WR 140 can be added to the short list of WR stars in

which freshly formed dust causes deep, relatively long-lasting eclipses (Crowther 1997; Veen et al. 1998; Kato et al. 2002). The very presence of small-scale structures in the winds prior to entrance into the WWC zone facilitates the dust formation by destabilizing the WWC zone and triggering fast radiative cooling (Walder & Folini 2002). We have already noted that the rapid appearance of the extra emission components in low-ionization lines favors radiative cooling as a cause. Thus, it is reasonable to expect that the freshly formed dust cloud could be broken (eventually or initially) into multiple clumps during the unstable cooling process. One cannot exclude the possibility that the numerous instabilities arising in the WWC interface (Stevens et al. 1992) could produce quasi-periodic spatial structures in the emerging cloud. Another possibility is clumps in the winds entering the collision zone. As a result of either, we may be observing a series of eclipse-like events (compare to Fig. 3) caused by a structured cloud crossing the line of sight. Note that the possible fragmentation of the WWC zone into layers (clumps?) of relatively cold, compressed gas not only creates the necessary conditions for dust formation (Cherchneff et al. 2000), but shields the newly formed dust from the harsh radiation field of the O and WR stars (Folini & Walder 2002).

We prefer to interpret the 2001 variability patterns as arising from the line-of-sight passage of freshly formed clouds of dust. The growth of variable amplitude toward the U band lends some additional support to this interpretation. Indeed, putting all the available UBV observations on the $(B-V)$ versus $(U-B)$ plane (Fig. 9), one can see that after entering the interval of rapid photometric variability, the star approximately follows the appropriate IS reddening line (cf. van der Hucht 2001 for the corresponding values). We assume that the intervening dust cloud is distant enough ($d > 10^2$ AU at $\phi > 0.03$) to occult both components. We select all the UBV data obtained during the period of rapid photometric variability, i.e., at $\phi = 0.020$–0.055, and assume that the variations are caused by the occulting clouds of mono-size amorphous carbon particles. Amorphous carbon is considered as a main constituent of the WR dust (Williams et al. 1987, 1990; Zubko 1998; Marchenko et al. 2002). To estimate the characteristic size of the dust particles, a, we calculate the weighted dust absorption coefficients $Q_{\rm abs}(\lambda, a)$ using Mie theory (Bohren & Huffman 1998) and optical constants for amorphous carbon (Zubko et al. 1996). The weights are calculated as $W(\lambda) = T(\lambda)F(\lambda)$, where $T(\lambda)$ is the transparency of the corresponding filter (U, B, or V) and $F(\lambda)$ is the energy distribution of WR 140 in the optical (Kuhi 1966). We link the observed photometric variability to changes of the circumstellar extinction $A(\lambda)$ and use the fact that $A(\lambda)$ is directly proportional to $Q_{\rm abs}$ (Spitzer 1978). Thus, the directly observable ratios of $A(U)/A(V)$ and $A(B)/A(V)$ (94 ratios in total) can be compared to the calculated ratios of $Q(U, a)/Q(V, a)$ and $Q(B, a)/Q(V, a)$, respectively, keeping the size a as the only parameter of the least-squares fit. Searching for a χ^2 minimum in the range of $a = 0.0001$–5.0 μm, we find a unique solution at $a = 0.069^{+0.002}_{-0.001}$ μm (95% confidence interval) with $\chi^2 = 243$ (93 degrees of freedom). The derived value of a, although somewhat lower than the recent estimates of particle sizes in the dust-forming WR stars WR 112 and WR 118, $a = 0.4$–1.0 μm (Chiar & Tielens 2001; Yudin et al. 2001; Marchenko et al. 2002), nevertheless points to a relatively large characteristic size of the particles, quite comparable to the sizes of presolar graphite spherules (e.g., Croat et al. 2002).

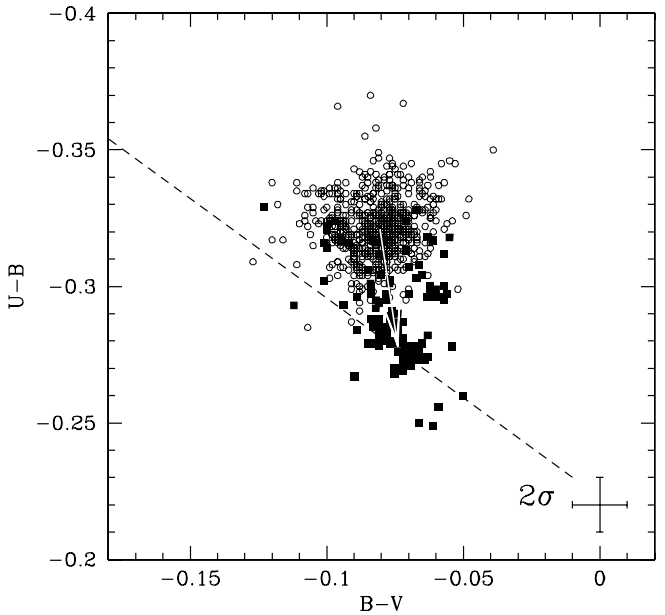

FIG. 9.—System's color variations. Open circles show the system in "quiescence"; filled squares mark the period of rapid photometric variability, HJD 2,452,000–2,452,100. The dashed line, displaced vertically by an arbitrary amount, follows the IS reddening line for WR 140. The arrow shows the increased intrinsic reddening trend during the 2001 event.

5. CONCLUSIONS

1. A new set of high-quality spectra taken during the 2001 periastron passage, combined with a complete set of other spectra over the whole orbit, allows us to obtain precise orbital elements for both components of WR 140 simultaneously and confirm the extremely high eccentricity, $e = 0.881 \pm 0.005$, among the highest known for massive binary systems. Assuming the orbital inclination of $i = 60°$, we find $M(\mathrm{WR}) = 19\ M_\odot$, $M(\mathrm{O}) = 50\ M_\odot$, $a = 16.3$ AU, and $a(1 - e) = 1.94$ AU.

2. The rapid rise and subsequent disappearance of an additional emission component in the low-ionization lines in the optical may signify that the wind-wind collision zone is governed by radiative processes during periastron passage. This would greatly facilitate the formation of dust. Application of the formalism of Lührs (1997) enables us to place some limits on the orbital inclination of the system, $i = 50° \pm 15°$, and half-opening angle of the bow shock cone, $\theta = 40° \pm 15°$.

3. It seems unlikely that the WR wind is highly flattened, since such flattening should result in a constant wavelength-independent ~3% component of the intrinsic polarization. Such a large signal should have been found in previous spectropolarimetric studies. The intrinsic polarization could be minimized by requiring a specific orientation of the flattened wind. However, this leads to a rather unlikely configuration, with the disk placed almost perpendicular to the orbital plane. Around periastron, the amplitude of the variable, phase-locked component of polarization is predicted to be about 0.1% (even slightly higher in the case of a flattened wind). This variable component should be detectable with a moderate-size telescope and a broadband photopolarimeter.

4. We interpret the series of occultation-like events at $\phi = 0.02$–0.06 as caused by freshly formed dust clouds. This allows us to estimate a characteristic size of the amorphous dust grains, $a \sim 0.07\ \mu$m.

We would like to thank D. Dimitrov for assistance in obtaining photometric observations in 2001 and Y. Hervieux for letting us use his large collection of 1989–1994 spectra. We also thank M. Blake, G. Caron, A.-N. Chené, S. Mochnacki, N. Morrison, and S. Rucinski for providing us with spectra of WR 140 taken in 2000/2001, at the critical times before and during periastron passage. We wish to thank V. Dwarkadas, K. Gayley, D. Folini, N. Morrison, J. Pittard, I. Stevens, R. Walder, and P. Williams for fruitful discussions and detailed comments. We also thank M. Seeds for coordinating the APT observations.

REFERENCES

Annuk, K. 1995, in Proc. IAU Symp. 163, Wolf-Rayet Stars: Binaries, Colliding Winds, Evolution, ed. K. A. van der Hucht & P. W. Williams (Dordrecht: Kluwer), 231
Bertiau, F. C., S. J., & Grobben, J. 1969, Ric. Astron. Spec. Vaticana, 8(1–2), 1
Bohren, C. F., & Huffman, D. R. 1998, Absorption and Scattering of Light by Small Particles (New York: Wiley)
Brown, J. C., Aspin, C., Simmons, J. F. L., & McLean, I. S. 1982, MNRAS, 198, 787
Brown, J. C., McLean, I. S., & Emslie, A. G. 1978, A&A, 68, 415
Cantó, J., Raga A. C., & Wilkin, F. P. 1996, ApJ, 469, 729
Cherchneff, I., Le Teuff, Y. H., Williams, P. M., & Tielens, A. G. G. M. 2000, A&A, 357, 572
Chiar, J. E., & Tielens, A. G. G. M. 2001, ApJ, 550, L207
Conti, P. S., Roussel-Dupre, D., Rensing, M., & Massey, P. 1984, ApJ, 282, 693
Croat, K., Bernatowicz, T., Stadermann, F. J., Messenger, S., & Amari, S. 2002, Lunar Planet. Sci. Conf., 33, 1315
Crowther, P. A. 1997, MNRAS, 290, L59
De Medeiros, J. R., Da Silva, J. R. P., & Maia, M. R. G. 2002, ApJ, 578, 943
Eenens, P. R. J., & Williams, P. M. 1994, MNRAS, 269, 1082
Folini, D. & Walder, R. 2002, in ASP Conf. Ser. 260, Interacting Winds from Massive Stars, ed. A. F. J. Moffat, & N. St-Louis (San Francisco: ASP), 605
Friend, D. B., & Abbott, D. C. 1986, ApJ, 311, 701
Harries, T. J., Hillier, D. J., & Howarth, I. D. 1998, MNRAS, 296, 1072
Hervieux, Y. 1995, in Proc. IAU Symp. 163, Wolf-Rayet Stars: Binaries, Colliding Winds, Evolution, ed. K. A. van der Hucht & P. W. Williams (Dordrecht: Kluwer), 460
Hill, G. M., Moffat, A. F. J., & St-Louis, N. 2002, MNRAS, 335, 1069
Hill, G. M., Moffat, A. F. J., St-Louis, N., & Bartzakos, P. 2000, MNRAS, 318, 402
van der Hucht, K. A. 2001, NewA Rev., 45, 135
van der Hucht, K. A., & Williams, P. W., eds. 1995, Proc. IAU Symp. 163, Wolf-Rayet Stars: Binaries, Colliding Winds, Evolution (Dordrecht: Kluwer)
Kato, T., Haseda, K., Takamizawa, K., & Yamaoka, H. 2002, A&A, 393, L69
Kuhi, L. 1966, ApJ, 143, 753
Lamontagne, R., Moffat, A. F. J., & Seggewiss, W. 1984, ApJ, 277, 258
Lührs, S. 1997, PASP, 109, 504
Maeder, A., & Meynet, G. 2000, ARA&A, 38, 143
Marchenko, S. V., Moffat, A. F. J., Vacca, W. D., Côté, S., & Doyon, R. 2002, ApJ, 565, L59
Moffat, A. F. J., Lamontagne, R., Williams, P. M., Horn, J., & Seggewiss, W. 1987, ApJ, 312, 807
Moffat, A. F. J., & Marchenko, S. V. 1993, AJ, 105, 339
Monnier, J. D., Tuthill, P. G., & Danchi, W. C. 2002, ApJ, 567, L137
Neutsch, W., Schmidt, H., & Seggewiss, W. 1981, Acta Astron., 31, 197
Panov, K. P., Altmann, M., & Seggewiss, W. 2000, A&A, 355, 607
Panov, K. P., & Dimitrov, D. 2001, Inf. Bull. Variable Stars, 5177, 1
Pollock, A. M. T., Haberl, F., & Corcoran, M. F. 1995, in Proc. IAU Symp. 163, Wolf-Rayet Stars: Binaries, Colliding Winds, Evolution, ed. K. A. van der Hucht & P. W. Williams (Dordrecht: Kluwer), 512
Pollock, A. M. T., et al. 2002, in ASP Conf. Ser. 260, Interacting Winds from Massive Stars, ed. A. F. J. Moffat & N. St-Louis (San Francisco: ASP), 537
Robert, C., Moffat, A. F. J., Bastien, P., St.-Louis, N., & Drissen, L. 1990, ApJ, 359, 211
Schulte-Ladbeck, R. E. 1994, Ap&SS, 221, 347
Setia Gunawan, D. Y. A., van der Hucht, K. A., Williams, P. M., Henrichs, H. F., Kaper, L., Stickland, D. J., & Wamsteker, W. 2001, A&A, 376, 460
Spitzer, L., Jr. 1978, Physical Processes in the Interstellar Medium (New York: Wiley)
Stawikowski, A., & Glebocki, R. 1994, Acta Astron., 44, 33
Stevens, I. R., Blondin, J. M., & Pollock, A. M. T. 1992, ApJ, 386, 265
St-Louis, N. 1996, Rev. Mexicana Astron. Astrofis. Ser. Conf., 5, 76
Usov, V. V. 1992, ApJ, 389, 635
Varricatt, W. P, Williams, P. M., & Ashok, N. M. 2003, Proc. IAU Symp. 212, A Massive Star Odyssey, from Main Sequence to Supernova, ed. K. A. van der Hucht, A. Herrero, & C. Esteban (Dordrecht: Kluwer), 253
Veen, P., et al. 1998, A&A, 329, 199
Walder, R., & Folini, D. 2002, in ASP Conf. Ser. 260, Interacting Winds from Massive Stars, ed. A. F. J. Moffat & N. St-Louis (San Francisco: ASP), 595
———. 2003, Proc. IAU Symp. 212, A Massive Star Odyssey, from Main Sequence to Supernova, ed. K. A. van der Hucht, A. Herrero, & C. Esteban (Dordrecht: Kluwer), 139
White, R. L., & Becker, R. H. 1995, ApJ, 451, 352
Whitney, B. A., et al. 1988, BAAS, 20, 738
Williams, P. M., van der Hucht, K. A., Pollock, A. M. T, Florkowski, D. R., van der Woerd, H., & Wamsteker, W. M. 1990, MNRAS, 243, 662
Williams, P. M., van der Hucht, K. A., & Spoelstra, T. A. Th. 1994, A&A, 291, 805
Williams, P. M., van der Hucht, K. A., & Thé, P. S. 1987, A&A, 182, 91
Young, A. I., et al., 1991, PASP, 103, 221
Yudin, B., Balega, Y., Blocker, T., Hofmann, K.-H., Schertl, D., & Weigelt, G. 2001, A&A, 379, 229
Zahn, J.-P. 1977, A&A, 57, 383
Zhekov, S. A., & Skinner, S. L. 2000, ApJ, 538, 808
Zubko, V. G. 1998, MNRAS, 295, 109
Zubko, V. G., Mennella, V., Colangeli, L., & Bussoletti, E. 1996, MNRAS, 282, 1321